Temperature Assisted Ligand Conversion from 3R-MoS_2 to α-MoO_3 by Preserving Layered Nature[#]

Manuja M*, Tintu Thomas and Gijo Jose

Post graduate and Research department of Physics S.B. College Changanasserry (Autonomous), Kottayam, Kerala, India

* E-mail: manuja.jayan85@gmail.com

Received: 20.9.2023, Revised: 20.1.2024, 27.1.24, Accepted: 27.1.24

Abstract

All polymorphs of 2D MoS_2 (1T, 2H & 3R) are layered with planes of molybdenum atoms sandwiched between two sulphur atoms (S-Mo-S layers) with intra planar covalent bonding and weak interlayer van der Waal's interactions. Here in this work, the role of polyethylene glycol as surfactant in the formation of 3R-MoS_2 is recognized. XRD and FTIR results provide structural elucidation and bonding information in the compound. More detailed crystal structure investigations and polyhedral visualizations were obtained in the Rietveld refinement procedure. The trigonal prismatic metal coordination in the 3R phase is portrayed with the ABC-ABC type layer stacking sequence. The morphology of layered 3R-MoS_2 nanostructure was identified from HRTEM images and the percentage composition from FESEM mapping and EDAX analyses. Temperature dependent mass loss in the compound is monitored and the quantitative analysis confirms the complete transformation of 3R-MoS_2 into layered α-MoO_3 at a temperature of 398 °C. Endo and exothermic peaks in the DSC and DTA measurements help to substantiate the results. Thus the work highlights the temperature assisted conversion of sulphide (3R-MoS_2) to oxygen ligand (α-MoO_3) of molybdenum at 398°C by cleavage of S-S bonds and preserving the layered nature.

Key words: 3R-MoS_2, layered nature, van der Waal's interaction, α-MoO_3, polyhedral structure.

Paper presented during 3rd International Conference on Recent Trends in Analytical Chemistry (26-28 June 23) organized by Department of Analytical Chemistry, University of Madras, Chennai and ISAS Tamilnadu Chapter

Introduction

Molybdenum dichalcogenides, for variety of applications has been grabbing the researcher'sincessant attentionin this day and age. MoS_2 can have the similar properties as that of graphite with an advantage of non zero band gap[1] and finds applications in diverse fields such as optoelectronics[2], energy storage systems[3], solar cells[4], FETs[5], switchable transistors[6], memristor devices[7] etc. Bulk MoS_2 is a diamagnetic[8], direct bandgap semiconductor[9] similar to silicon, with a bandgap of 1.23 eV. MoS_2 exists in three phases 1T, 2H and 3R phases. All forms have a layered structure, in which a plane of molybdenum atoms is sandwiched by planes of sulphide ions. 1T phase is metastable with a solitary layer and the basic building block is an octahedron. But in 2H and 3R phases the basic building block is a trigonal structure with two and three sorts of layers respectively[10]. The intra-planar connection is dominated by covalent bonding and the inter-planar bonding is very weak vander Waal's interactions[11].

The layered nature of MoS_2 can be exfoliated even to monolayer form using scientific methods. The exfoliation will accompany the change in band gap and the luminous intensity in photoluminescent spectra[12]. The layered structure enables foreign cations to intercalate in between the layers and tunes the optical and electrical properties via structural distortion and band gap tailoring[13]. This work highlights the conversion of ligands associated with molybdenum atoms by providing heat treatment and the importance of these findings vest in the preservation of layered nature even after the change of ligands at high temperatures. The 3R-MoS_2 having trigonal prismatic co-ordination structure is transformed to octahedral geometry in α-MoO_3 during temperature treatment with accompanied oxidation. At the meantime the centre of symmetry of two compounds also changes. 3R-MoS_2 lacks center of symmetry and α-MoO_3 is centrosymmetric in structure. The change in symmetric structure can impose temperature stimulated electric phase transition in the compound thereby allowing conductivity tuning. Hence ligand conversion has importance in the present study even there is direct procedure for the production of layered α-MoO_3.

Experimental techniques

Sample preparation

The hydrothermal techniques were used to synthesize powdered 3R-MoS_2 from sodium molybdate ($Na_2MoO_4.2H_2O$-AR grade) and thiourea (NH_2CSNH_2-AR grade) in presence of

HCl/polyethylene glycol. 0.2 M and 0.6 M solutions of sodium molybdate and thiourea were prepared and mixed with 30 ml of diluted HCl with continuous stirring at 80 °C for half an hour. The resulting precursor solution is transferred to teflon lined stainless auto clave at 140 °C for 6h, 8h, 11h in three trials. The temperature increased to 200 °C and kept in an autoclave for 11h in the fourth trial.Again the acidic medium of HCl is replaced by polyethylene glycol and the process is repeated with 1.21g sodium molybdate, 1.56 g thiourea and 0.14 g polyethylene glycol in fifth trail. All samples were centrifuged several times using water and ethanol and dried in an oven at 80 °C for 3 h.

Characterization techniques

Structural confirmation of the prepared samples were done using powdered x-ray diffraction techniques (XRD) in Bruker D8 x-ray diffractometer having $CuK\alpha_1$ (λ=1.5406 Å) radiation with step size of 0.02 and a scan rate of 3º per minute between 2θ values ranges from 5 to 65º.The Rietveld refinement procedure of x-ray diffraction profiles for detailed investigation of structure and getting bonding information were done in fullprof suit. Further structural confirmations were done in FTIR analysis and were recorded using 'Perkin-Elmer' spectrum 2 with in a wavenumber range of 400 to 4000 cm^{-1}.The morphology was visualized from FESEM and HR-TEM images from Versa 2D dual beam analyzed equipped with EDAX and Tecnai G2T20 instrument FEI, Netherlands respectively. Thermo gravimetric analysis (TGA) and differential scanning calorimetry (DSC) were performed in SDTQ600.Thermogravimetric analyzer provides simultaneous measurement of mass change and differential heat flow on the same sample. Both measurements were taken with a heating rate of 20 ºC/minute within temperature range from 30 to 700ºC.

Results and Discussion

The samples collected were analyzed for its structural properties and phase purity by non destructive x-ray diffraction techniques at room temperature. Recorded PXRD profiles are displayed in Fig.1 (a). The figure compares and identifies the importance of polyethylene glycol in the synthesis technique. Fig. (1a) (i-iv) represents the diffracted PXRD profiles of samples prepared without polyethylene glycol at different processing temperature and time. The dominating peak at 2θ=14° becomes sharper with the rise in temperature and processing time. With the presence of polyethylene glycol as surfactantFig. 1a (v) plot shows more

diffraction peaks at different 2θ vales at 13.69°, 32.85°, 35.61°, 42.3° and 57.54° and could beindexed to (003), (101), (012), (015), and (110) planes. This corresponds to rhombohedral phase of MoS_2 as signified in Fig.1(b) along with the ICSD details at the bottom. The peaks in the spectra are confirmed without any impurities and is used for the further analysis throughout the work.

For getting further details regarding polyhedral structure refinement of XRD profiles are carried out and bonding details are analyzed. The Rietveld refinement enlights more detailed crystal structure when refined in fullprof suit. The least square approach is adopted for refining the recorded data to match with theoretical profiles. Psedovoigit function in a linear combination of Gaussian and Lorentzianfunctions[14,15] is used for the better refinement following the relation,

$$y_{(x)} = V_p(x) = n * G(x) + (1 - n) * Ln(x). \quad (1)$$

The refined output corroborate R3m(160) space group in rhombohedral geometry with 3m point group having Wyckoff sequence a3 and Pearson code hR3. The lattice parameters a=b=3.1069Å and c=19.0300Å matches well with the theory and prior findings with c/a ratio 6.1251 Å. Higher c/a identifies the layer stacking with van derWaal's interaction along '**c**' axis and is indicated in Fig. 2 (a). In rhombohedral MoS_2 (3R-MoS_2) the basic building block is trigonal prismatic coordination sphere with Mo (IV) occupies at the centre and each molybdenum atoms is surrounded by six sulphur ligands. The bond length details and the fundamental structuresare shown in Fig. 2(b-c). Each Mo-S bond is equal with a distance of 2.5243 Å where sulphur atom again is the centre of a pyramid and is connected to three Mo atoms with formula sum Mo_3S_6 which reconcile with previous reports. The atomic (distance between centre of nucleus and outermost shell of an atom[16]), ionic[17] and vander Waal's radii[18]of Mo/S atoms in the compound are 1.4/1.04, 0.59/1.84 and 2.02/1.8 Å respectively. The higher the ionic radius, larger will be the spread of electron configuration in space and greater the tendency to polarize[19]. Hence the foreign ions having sufficiently lower ionic radius of Na^+ (1.02)[20], Li^+ (0.74), and Mg^{2+} (0.72) can be used to intercalate into the vacant site thereby improve the electric properties[21].

The intraplanar covalent bonding exists in each MoS_2 bc planes and they are connected between two sulphur atoms by van der Waal's interaction along c axis originatingthe layered nature. Thus c/a ratio gets a higher value. In the layered structure, each Mo atoms are sandwiched between two layers of sulphur atoms. Basic layer is similar to the structure of 2H

MoS_2 but in 3R structure each fourth layer is the repetition of first layers giving ABC-ABC layer stacking sequence thereby forms 3 different orientations along ab planes giving 3R structure. The symmetry operations and bravais sites obtained from the output pattern are *x,y,z; y,x-y,,z;-x+y,-x,z; -x+y,y,z; x,x-y,,z; and –y,-x,z* with bravais sites (0,0,0), (2/3,1/3, 1/3) and (1/3, 2/3, 2/3).

A deeper insight into inter and intra layer bonding were obtained from more sensitive FTIR observations as recorded in Fig. 3 within the wavenumber range of 400 to 4000 cm^{-1}. In addition to the peaks representing presence of water and O-H group at 3452and 3162 cm^{-1} respectively[22], there are 4 other prominent peaks at 540, 931, 1083 and 1424 cm^{-1}. The first two peaks correspond to Mo-S and S-S bonding present in layered 3R-MoS_2[23,24]. This represents the presence of covalent bonding between Mo and S and the interlayer van der Waal's interaction between sulphur ligands. This peak substantiates for the existence of layered nature in the compound. Next two peaks at 1083 and 1424 cm^{-1} stands for the presence of polyethylene glycol, and $–CH_2$ stretching modes associated with the surfactant[25,26]. A very small shoulder peak at 826.4 cm^{-1} specifies the oxidation occurring on the surface level of sulphur ligands on MoS_2[27].

FESEM micrographs of rhombohedral MoS_2 are given in Fig. 4 (a) and disclose the agglomerated image of samples. The agglomeration makes the identification of proper morphology a tedious task however; the histogram represents the size distribution of the particle in the nano meter range. The nanostructure within the radius range of 60-80 nm shows maximum distribution and is indicated in the inset of Fig. 4 (a). HRTEM images played a role for more clear visibility of morphology and identification of growth direction. A single enlarged view of crystal is seen in Fig. 4 (b) identifies the 2D nanoflake like structure with thickness confined to 8 nm in dimension and the length x breadth is 174 × 145 nm. The attractive feature of the morphology lies in the transparent nature of samples with presence of pore sizes. Some of the pores are marked circularly in the respective image. The pore size has a diameter of about 9.43 nm and this can act as a host for foreign materials to root on the surface.

The morphology and its peculiar nature lead to vital applications of energy storage mechanisms[28]. Lattice fringe pattern is given in Fig. 4 (c) shows incomplete layers but confirms d spacing of 0.6 nm indicating the (003) planes. The fringe pattern again clarifies the c directional layer stacking and the growth direction. SAED pattern tells about the

polycrystalline structure in Fig. 4 (d). FESEM mappings function as a supportive evidence for the identification of composition of elements present in the compound, along with EDAX results. The mapping of composition for the elements present in the highlighted region of Fig. 5(a) is shown in Fig. 5 (b-d). The inset of Fig. 5(b) gives the EDAX observations. The percentage composition of molybdenum and sulphur is identified as 1:2.33 in the typical compound. The non stoichiometry arises due to the incomplete growth of the sample during this processing time and temperature, as substantiated from lattice fringe patters. The presence of both Mo^{4+} and Mo^{6+} are identified with a ratio of Mo^{6+}/Mo^{4+} as 1.02[29]. Existence of this non stoichiometric molybdenum takes the role of several unique electrical and optical properties in the typical compound and provides stability for the compound.

order to identify the thermal stability of the prepared material thermo gravimetric analysis was carried out. In TGA (Fig. 6 (a)), provides percentage massloss as a function of temperature. For the sake of explanation, the total region of TGA is divided into four sections. In the first region (from room temperature to 102 °C) there is a mass loss of 6.9 % which corresponds to the removal of absorbed water from the compound associated with the hygroscopic nature of typical material. The region II (102 °C to 331 °C) shows a mass loss of 6.02%. The third region III (331 °C to 398 °C) suffers a mass loss of 5.2 % associated with the complete modification of 3R-MoS_2 to α-MoO_3. Higher temperature constancy of TGA plot indicates the stability of α-MoO_3 with respect to temperature. The removal of absorbed water from the compound at 102 °C is confirmed by an endothermic peak in DSC and DTA plots as represented in Fig. 6 (b).

As elucidated from the thermal analyses MoS_2 is annealed at 398 °C and room temperature PXRD result is verified. The orthorhombic (α) phase of MoO_3 is obtained. The phase pure and impurity free samples are identified from PXRD profiles and the peaks are indexed as shown in Fig.7. The standard JCPDS values are attached at the bottom for comparison. Presence of (0 2 0), (0 4 0), (0 6 0) and (0 10 0) identifies the growth of α-MoO_3 along {0 k 0} phase sets. The growth along the b axis is the clear indications of layered nature with inter layer van der Waal's interaction along the 'b' axis and the intralayer covalent bonding along the ac plane. Thus planar layer grows along the ac plane forming lamellar structure and the layer stacking occurs along the b axis as indicated in Fig.8 which represents Rietveld refined output of α-MoO_3. In addition, α-MoO_3 structure is formed from MoO_6 octahedra with Mo atom at the centre and surrounded by six oxygen atoms with three types of position specifications. The detailed structure of layered α-MoO_3 and its exfoliation techniques for the

reduction of layered number is discussed in our previous publication[30]. The basic building block is octahedra MoO_6 as indicated in Fig.8. With the increase in temperature S-S bond gradually gets cleavage and new bonds are formed between Mo and O and it completely get transforms to α-MoO_3 at 398 °C while preserving layered nature.

Further confirmation of the processing time of MoS_2 preparation is done again by repeating the sample synthesis technique with polyethylene glycol for 24 h. The PXRD profiles are shown In Fig.9. The well defined peaks show the more oriented samples with the same growth direction (003) along c axis.

Conclusions

The hydrothermal synthesis of 3R-MoS_2 depends strongly on the presence of surfactant (polyethylene glycol), the processing time and the temperature. 3R-MoS_2 has layered nature with ABC-ABC stacking and fourth layer is the repetition of first layer. The layered nature arise due to the weak van der Waal's interaction between inter layer sulphur atoms. The growth direction and the layer stacking is along 'c' axis. Molybdenum is multivalent in the typical compound and the nonstoichiometry arises due to incomplete growth. With the increase in temperature S-S bonds breaks and new bonds form by the oxidation and the formation of Mo=O. Thus 3R-MoS_2 completely transforms to α-MoO_3 at 398 °C with the retention of layered nature and the growth is along 'b' axis.

Acknowledgement

MM acknowledges the financial support provided by Kerala Startup mission and KSUM, MG University (RINP 2022).

Figures:

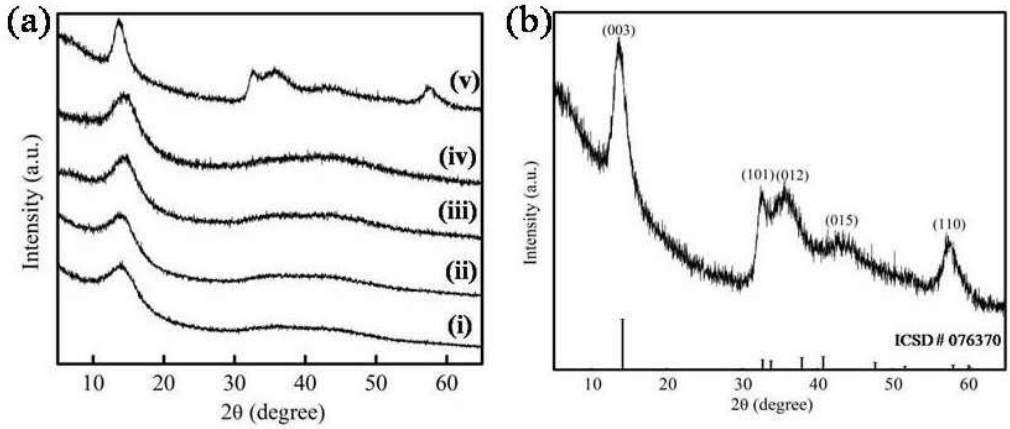

Fig. 1 (a) X-ray diffraction profiles of 3R-MoS_2 with different conditions of preparation (a-d) without polyethylene glycol at different processing time and temperature and (e) with polyethylene glycol. (b) The enlarged plot for 3R-MoS_2 with ICSD profiles at the bottom

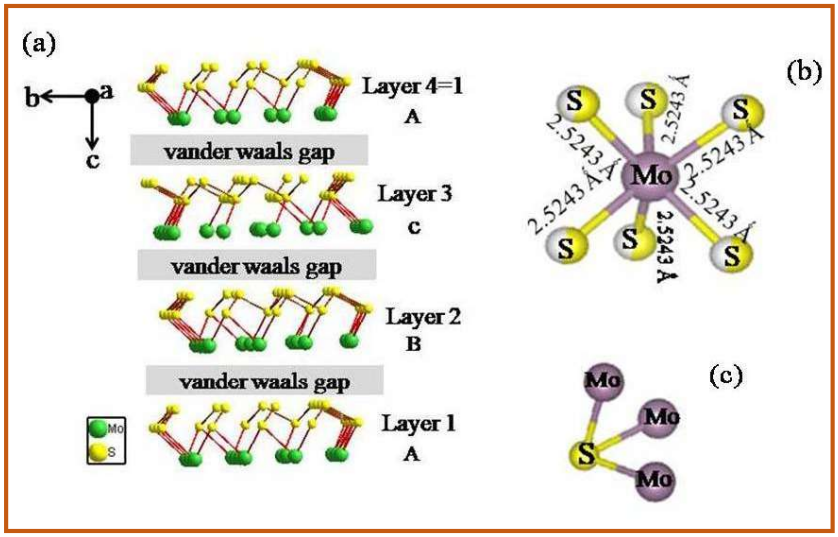

Fig. 2Reitveld refined structure of 3R-MoS_2(a) clearly identifying the layered nature and stacking sequence (b) basic crystal structure of trigonal geometry with Mo at the centre and (c) with S at the centre

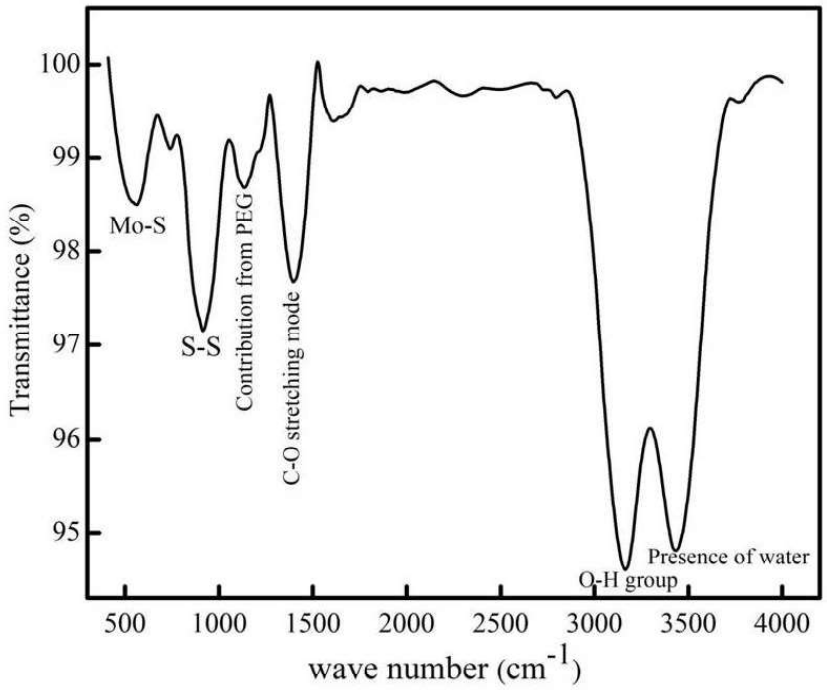

Fig. 3 FTIR spectra of 3R-MoS_2 with the wave number range 400 to 4000 cm^{-1}

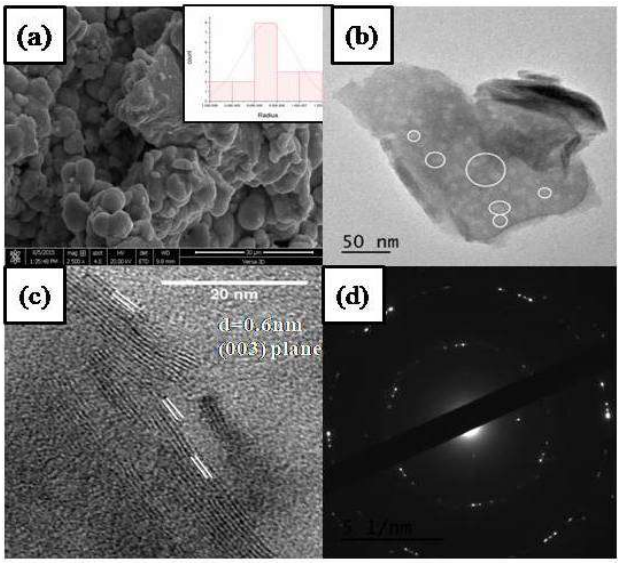

Fig. 4 Electron microscopy images of 3R-MoS_2 (a) FESEM images with histogram at the insets, (b) HRTEM image of a single particle morphology, (c) lattice fringe pattern and (d) SAED pattern .

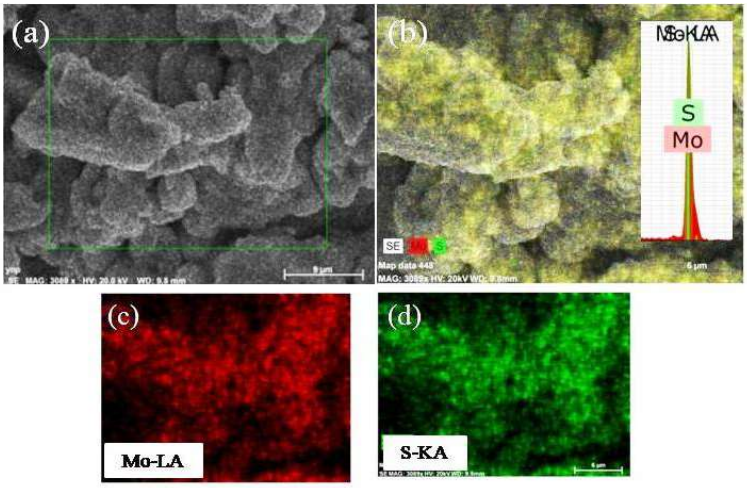

Fig. 5 FESEM mapping mages of 3R-MOS_2 (a) FESEM image, (b) mapped image with Mo and S presence of (c) Mo identification image and (d) S identfication image.

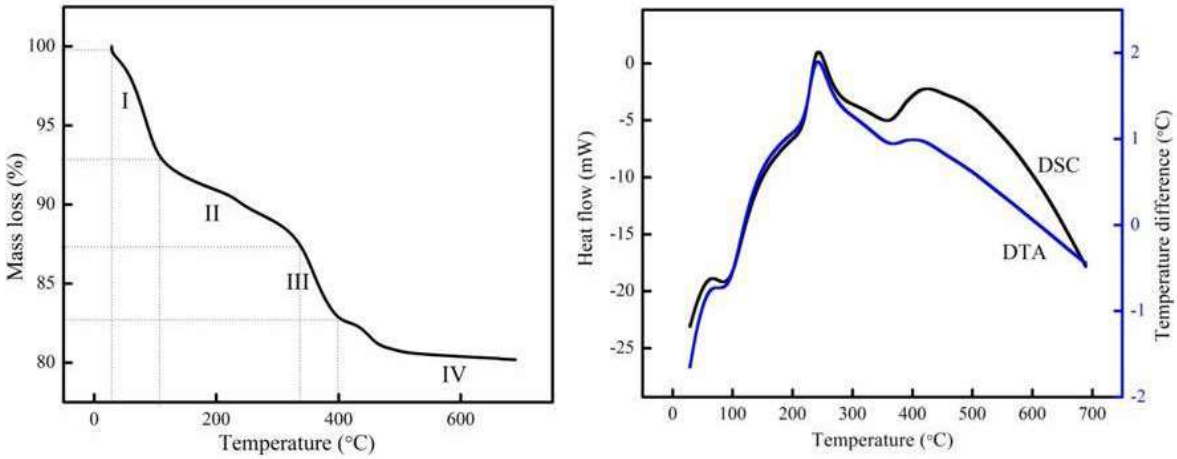

Fig. 6 Thermogravimetry analysis of 3R-MoS_2 (a) TGA indicating percentage mass loss with respect to temperature and (b) DSC and DTA plots of 3R-MoS_2

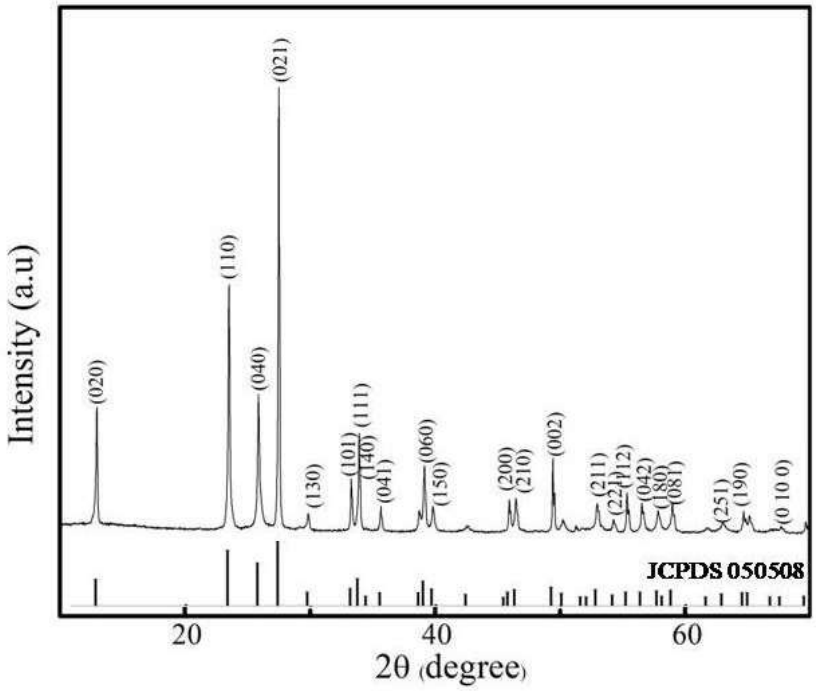

Fig. 7 X-ray diffraction patterns for layered α-MoO_3 with corresponding JCPDS data at the bottom.

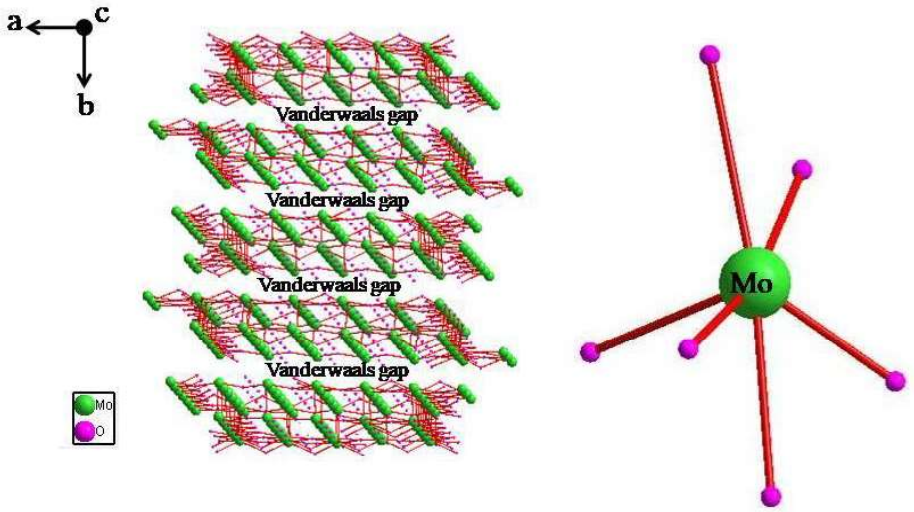

Fig. 8Reitveld refined image of α-MoO_3 indicating layered nature and stacking sequence with the basic building blocks of octahedral structure with Mo at the centre.

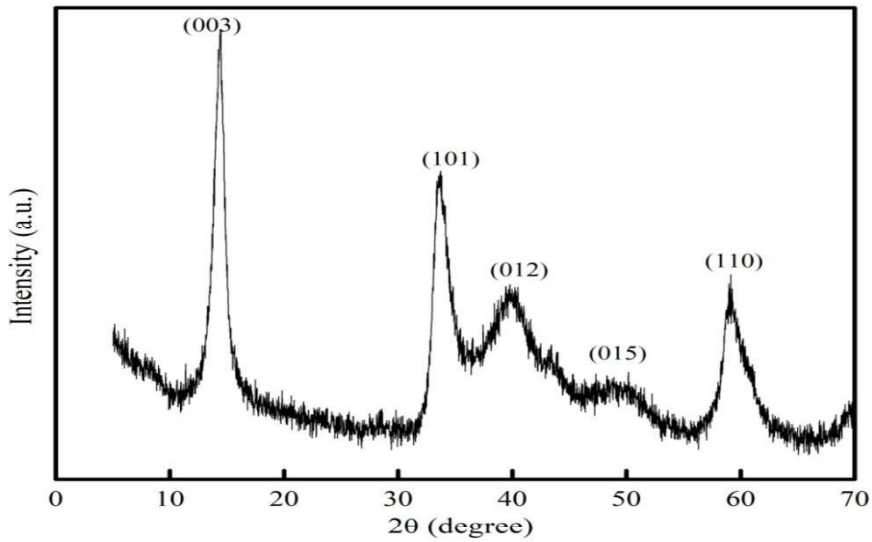

Fig. 9 X-ray diffraction profiles of 3R-MoS_2 with well defined peaks when PEG used as and processed at 24 h time

References

1. X. Li, and H. Zhu, *J.Materiomics*, *1(1)*, 33, 2015.
2. T. Nawz, A. Safdar,M. Hussain, D. S Lee, and M. Siyar, *Crystals.*, *10(10)*, 902, 2020.
3. T. Wang, S. Chen, H. Pang, H. Xue, and Y. Yu, *Adv. Sci.*, *4(2)*, 1600289,2017.
4. U. Dasgupta, S. Chatterjee, and A. Pal, *J. Sol. Energy Mater Sol. Cells.*, *172*, 353, 2017.
5. C. Wang, Y. Song, andH. Huang, *Nanomater.*, *12(18)*, 3233, 2022.

6. Y. Zhao, S. Bertolazzi, M. S. Maglione, C. Rovira, M. M. Torrent, andP. Samorì, *Adv. Mater.*, *32(19)*, 2000740, 2020.
7. Y. Gu, M. I. Serna, S. Mohan, A. L.Calderon, T. Ahmed, Y. Huang, and D. Akinwande, *Adv.Electron. Mater.*, *8(2)*, 2100515, 2022.
8. Mathew, S., Gopinadhan, K., Chan, T. K., Yu, X. J., Zhan, D., Cao, L., and Thong, J. T. *Appl. Phys. Lett.*, *101*, 2012.
9. N. Thomas, S. Mathew, K. M. Nair, K. O. Dowd, P. Forouzandeh, A. Goswami, and S. C. Pillai, *Mater. Today Sustain.*, *13*, 100073, 2021.
10. M. Manuja, andG. Jose, *Research Aspects in Chemical and Materials Sciences, BP international 5*,2022.
11. S. W. Han, H. Kwon, S. K.Kim, S. Ryu, W. S. Yun,D. H. Kim, andS. C. Hong, *Phys. Rev. B*, *84(4)*, 045409,2011.
12. M. Manuja, T. Thomas, andG. Jose, In *IOP Conf. Ser.: Mater. Sci. Eng.* IOP Publishing 1263(1), 012021,
13. M. Manuja, and G. Jose, *Fundamental Research and Application of Physical Science, B.P international2*, 2023.
14. M. Manuja, T. Thomas, J. Jose, G. Jose, andK. C. George, *J. Alloys. Compd.*, *779*, 15, 2019.
15. M. Manuja, K. V. Sarath, T. Thomas, J. Jose, andG. Jose, *J. Electron. Mater.*, *49*, 2556, 2020.
16. P. Yadav, H. Tandon, B. Malik, V. Suhag, andT. Chakraborty, *Struct. Chem.*, 33, 389, 2022.
17. K. Hayamizu, Y. Chiba, andT. Haishi, *RSC adv.*, *11(33)*, 20252, 2021.
18. .P. Luo, C. Liu, J. Lin,X. Duan, W. Zhang,C. Ma, andX. Liu, *Nat. Electron.*, *5*, 849, 2022.
19. A. M. O. Mohamed, E. K. Paleologos,Fundamentals of Geoenvironmental Engineering, Butterworth-Heinemann,Elsevier 205 2018.
20. M. Goswami, S. Kumar, H. Siddiqui, V. Chauhan, N. Singh,N. Sathish, andS. Kumar, In *Emerging Trends in Energy Storage Systems and Industrial Applications,* Academic Press, 223 2023.
21. V. W. Fisher, J. M. Delgado, P. R. Nagy, E. Jakobsson, S. A. Pandit, andS. Varma, *J. Chem. Phys.*, *153(10)*, 104113, 2020.
22. K. C. Lalithambika, K. Shanmugapriya, andS. Sriram, *Appl. Phys. A*, *125*, 1,2019.

23. S. Liu, X. Zhang, H. Shao, J. Xu, F. Chen, andY. Feng, *Mater. Lett.*, *73*, 223, 2012.
24. K. C. Lalithambika, K. Shanmugapriya, andS. Sriram, *Appl. Phys. A.*, *125*, 1, 2019.
25. A. R.Polu, and R. *E.* Kumar, *J. Chem.*, *8(1)*, 347,2011.
26. S. Liu, X. Zhang, H. Shao, J. Xu, F. Chen, andY. Feng, *Mater. Lett.*, *73*, 223, 2012.
27. T. He, andJ.Yao, *JPPC., 4(2)*, 125, 2003.
28. M. Manuja, T. Thomas,S. John, J. Jose, andG. Jose, *J. Alloys.Compd.*, *869*, 159234, 2021.
29. M. Manuja, K.V. Sarath, and G. Jose, *IOP Conf. Ser. Mater. Sci. Eng.* IOP Publishing, pp012015,October 2018
30. M. Manuja, T. Thomas, J. Jose, andG. Jose, *Mater. Today. Proc.*, pp5283, 2022.